Determination of elastic properties of polycrystalline U_3Si_2 using resonant ultrasound spectroscopy

U. Carvajal-Nunez [a], *, T.A. Saleh [b], J.T. White [b], B. Maiorov [c], A.T. Nelson [b]

[a] Center for Integrated Nanotechnologies, Los Alamos, 87545, NM, USA
[b] Materials Science and Technology Division, Los Alamos National Laboratory, Los Alamos, 87545, NM, USA
[c] Materials Physics and Applications Division, Los Alamos National Laboratory, Los Alamos, 87545, NM, USA

A B S T R A C T

The elastic properties of U_3Si_2 at room temperature have been measured via resonant ultrasound spectroscopy. Results show that the average value of Young's and the bulk modulus for U_3Si_2 are 130.4 ± 0.5 and 68.3 ± 0.5 GPa, respectively. Further, a numerical model to assess thermal stress in an operating fuel is evaluated. The thermal stress evolved in U_3Si_2 is compared to UO_2 to facilitate an estimation of the probability of crack formation in U_3Si_2 under representative light water reactor operating conditions.

© 2017 Published by Elsevier B.V.

1. Introduction

Uranium silicides are being proposed as an alternative fuel for Light Water Reactor (LWR). The increase in uranium density and improved thermal conductivity compared to UO_2 has increased interest in uranium silicides as nuclear fuels in next generation reactors. Among uranium silicon compounds, U_3Si_2 is the leading candidate due to its properties such a high uranium density, high thermal conductivity, high melting temperature and existing data from irradiation testing [1,2]. However, other uranium silicon compounds are also of interest for comparison and understanding the U-Si fuel system.

Measurement of the thermophysical and thermodynamic properties of these constituent materials has advanced in recent years [3—6], but evaluation of mechanical properties at room and relevant temperatures observed in a reactor is necessary to support further evaluations. While thermophysical properties such as thermal conductivity, heat capacity, and thermal expansion are generally the primary properties of interest for assessment of an actinide compound for nuclear fuel service, mechanical properties will play an important role in governing the deformation and fracture of the fuel during both normal operation and potential transients [7]. It is therefore necessary to evaluate these elastic properties, to predict the response of a candidate fuel form to anticipated thermal gradients.

Measurement of mechanical properties of conventional ceramic and intermetallic nuclear fuel materials is challenged by the fact that brittle failure dominates practical relevance at low temperatures. Evaluation of brittle failure in ceramics requires comprehensive investigation and specific test specimen geometries. The cost of such test campaigns is often prohibitive when judged against the relative importance of mechanical properties on fuel performance and evolution in mechanical properties anticipated during irradiation and burnup. However, basic elastic constants are necessary not only as basic inputs into fuel performance codes but also as benchmarks to first principles modeling efforts. Elastic behavior of unirradiated and irradiated nuclear fuels have been explored to a limited extent using conventional mechanical testing techniques [8—14] such as scanning acoustic microscope or longitudinal ultrasonic velocity techniques.

One of the material properties targeted for improved performance of nuclear fuels is the thermal stress resistance [15], which is generated when the expansion of the heated body is restrained. This behavior manifests as fuel pellet cracking. UO_2 pellets

operating under reactor conditions typically develop large radial cracks in their outer regions [16]. The thermal stress in a cylindrical specimen under elastic strain behavior is governed by its thermal expansion, thermal conductivity, linear heat generation and elastic modulus [17]. While recent experimental work has measured the thermal conductivity and thermal expansion of U_3Si_2 as a function of temperature, elastic properties measurements of its elastic properties are limited to historic investigations performed during initial exploration of U_3Si_2 as a nuclear fuel. U_3Si_2 as prepared historically is often reported to contain a significant fraction of impurity phases, non-uniformities, cracks and chemical and structural characterization are generally absent in archival reports. Further, the limited existing vary widely. Improved elastic values is therefore necessary to facilitate even basic assessment of the thermal stresses anticipated in a U_3Si_2 fuel pellet during operation.

Resonant ultrasound spectroscopy (RUS), a non-destructive technique, can provide an alternative to other traditional mechanical testing methods [18,19]. The technique is useful for measurement of the elastic properties of the bulk structure of various materials and different compositions. RUS measurement generates mechanical full body resonance spectrum [20−22]. From this spectrum, an inversion scheme can be used to extract the elastic moduli.

In this study, RUS is used to determine the basic mechanical properties of high density U_3Si_2. The independent elastic constants C_{11}, C_{44} and the bulk modulus have been evaluated to calculate the Young's modulus and the Poisson's ratio. This data then allows for initial assessment of the thermal shock resistance of U_3Si_2, and compare it to the reference UO_2 nuclear fuel.

2. Experimental

2.1. Sample preparation and characterization

U_3Si_2 samples were prepared using a powder metallurgy process reported by White et al. [4]. The resulting samples following milling and sintering of the arc melted material were between 92 and 95% of the theoretical density taken as 12.2 g/cm^3 U_3Si_2 [23]. High density UO_2 was fabricated using material and processing conditions identical to those reported elsewhere [24]. Samples were stored in glovebox under inert atmosphere to minimize oxidation. Since shape irregularity samples will produce discrepancies in the frequency response, careful measurement dimension was performed to determine the geometry of all samples tested. For all samples in this study, for an increase in diameter of 0.07 mm the resonance frequencies are slightly shifted by approximately 0.7 kHz. The dimensional variations for all pellets used in this study were no greater than 0.05 mm and generally below 0.02 mm. Surface roughness (r_a) measurements collected for faces of similarly prepared and processed pellets provide values between 0.005 and 0.015 mm. The minimum shift in frequencies found by varying

the dimensions to this extent demonstrates that geometries of the variability used in this study will not degrade the measurements.

Dimensions of all pellets are reported in Table 1. The balance used to determine masses in this study was calibrated to 0.01 mg. Diameter and length were recorded with a digital caliper and calibrated to 0.01 mm. Seven U_3Si_2 specimens from set A (samples 1−5) and sample set B (samples 6−7) were synthesized from different feedstocks chosen to explore the potential effect of impurity phases on mechanical properties for this material. Besides U_3Si_2 samples two U_3Si_5 pellets were synthesized using the procedure reported by White et al. [6].

XRD performed on the sintered samples provided information regarding phases present. For the XRD measurements, the powder was mounted on a Si crystal zero-background plate using a thin layer of vacuum grease and then sealed inside a polymer dome while inside the glovebox. The polymer dome had an air scatter shield installed to minimize the contribution of the background to the signal. Powder samples were prepared by milling in a mortar inside an Ar atmosphere maintained below 30 ppm O_2 concentration to minimize oxidation of the powder.

XRD measurements was carried at room temperature then analysis using a Bragg-Brentano Bruker (D2 Phaser, Bruker AXS, Madison, WI, USA) diffractometer using Cu Kα radiation. The powder patterns were recorded by step scanning using a step size of 0.01° with and exposure of 3 s across the angular range 20°$\leq 2\theta$ $\leq 90°$.

Typical XRD pattern for U_3Si_2 set A and B are displayed in Fig. 1. According to the XRD patterns presented in Fig. 1, peaks derived
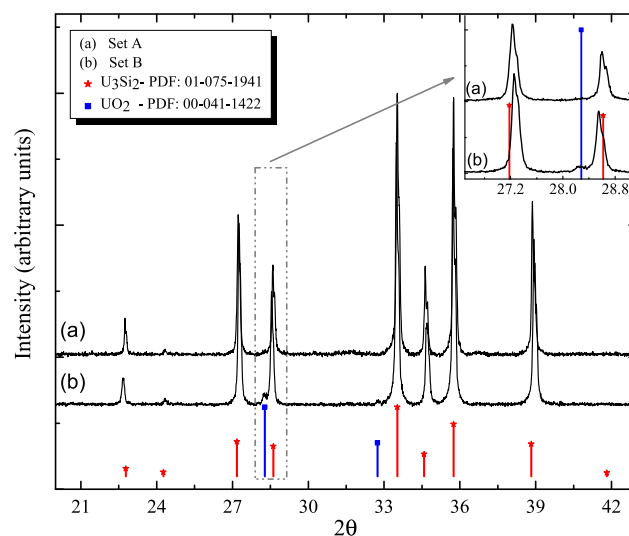

Fig. 1. Comparison of the XRD patterns for a representative sample of set A (a) and B (b). Reference files are from: 01-075-1941 (U_3Si_2) [25] and 00-041-1422 (UO_2) [45].

Table 1
Summary of the specimen geometry and density as measured. Density for U_3Si_2 B samples is calculated assuming 1.4 vol percent UO_2.

Material	Sample ID	Mass [g]	Diameter(D) [mm]	Length(L) [mm]	D/L	Density [g/cm^3]	Theor. density %
U_3Si_2, A	1	0.9952	4.76	4.84	0.98	11.55	94.7
	2	0.8929	4.76	4.33	1.09	11.59	95.0
	3	0.9204	4.76	4.47	1.06	11.57	94.9
	4	1.0529	4.76	5.12	0.92	11.56	94.7
	5	0.9006	4.76	4.38	1.08	11.55	94.7
U_3Si_2, B	6	0.9923	4.83	4.79	1.00	12.72	92.7
	7	1.0325	4.78	5.48	0.87	12.56	91.6
UO_2	8	0.6465	4.37	4.10	1.06	10.51	95.9

from the P4/mbm U_3Si_2 structure are observed [25] (see legend Fig. 1). Thus, for U_3Si_2 set B, UO_2 phase is identify in the XRD pattern.

SEM analysis was also used to investigate the microstructure of the synthesized specimens. Polished surfaces of the samples were analyzed using a Phenom ProX SEM (Phenom World, Amsterdam, Netherlands) equipped with backscatter and Electron Dispersion Spectroscopy (EDS) detectors. Specimens were cross sectioned and embedded in epoxy. Then, samples were ground and polished using silicon carbide papers and polishing cloths, with the final polish performed using 0.05 μm-alumina dispersion. Fig. 2 shows an SEM image of U_3Si_2 set B. Although the majority of the cross sectioned surface for both set of samples was identified as a single phase, one secondary phase was observed in set B using electron backscatter detection. For U_3Si_2 specimens, EDS measurements confirmed that this secondary phase is UO_2. UO_2 inclusions are a typical impurity phase present in U_3Si_2 as fabricated from arc melting and powder metallurgy given the rapid oxidation of U_3Si_2 powders even when stored under controlled environments [1,4]. For U_3Si_2 set A, the precipitates are observed as 5—10 μm. These precipitates constituted less than one volume percent as established by the microstructural analysis technique. Digital image analysis by ImageJ software [26] of 10 SEM images allowed quantification of the secondary oxide phase fraction. Results indicates that UO_2 phase is present at approximately 1.4±0.4 vol percent in the U_3Si_2 set B. As anticipated by XRD results, samples prepared from set B confirmed the presence of UO_2.

Samples produced from feedstock U_3Si_2 set B were therefore included in this study to assess the effect of UO_2 content on the measured mechanical properties of given the likehood or high probability of its presence as an impurity phase in U_3Si_2 produced at large scale.

2.2. Resonant ultrasound spectroscopy (RUS)

Fig. 3 shows the experimental configuration used in this study to measure the mechanical resonant spectrum. The photograph highlights a cylindrical sample held between hemispherical Al_2O_3 glued to the transducer. Transducers operated in the 1—10 MHz range for all experiments performed in this study.

RUS measurements were collected at constant amplitude using a National Instrument NI, PXIe 1075 function generator. Both generation and acquisition lines are managed by the Resonance Inspection Techniques and Analysis (RITA©) a software package developed at Los Alamos National Laboratory (LANL) [27]. For the U_3Si_2, the driving frequency ranged from about 300 to 500 kHz. Dimensions and masses used in the analysis are given in Table 1. For the validation of RUS set up, an Al 4% Cu standard sample is used as reference material for the resonance frequency measurements. Corners of the sample are positioned in the transducers preventing points of symmetry to avoid nodal location for the low lying modes [27]. Fig. 4 shows a typical spectrum obtained for the U_3Si_2 samples in comparison with the predicted resonace peaks, from the resulted moduli.

Elastic constants were calculated from the spectrum using the Rayleigh-Ritz method. The method is an inverse process, where the elastic moduli are calculated from the resonance frequencies. The solution of the mathematical model depends on the dimension and
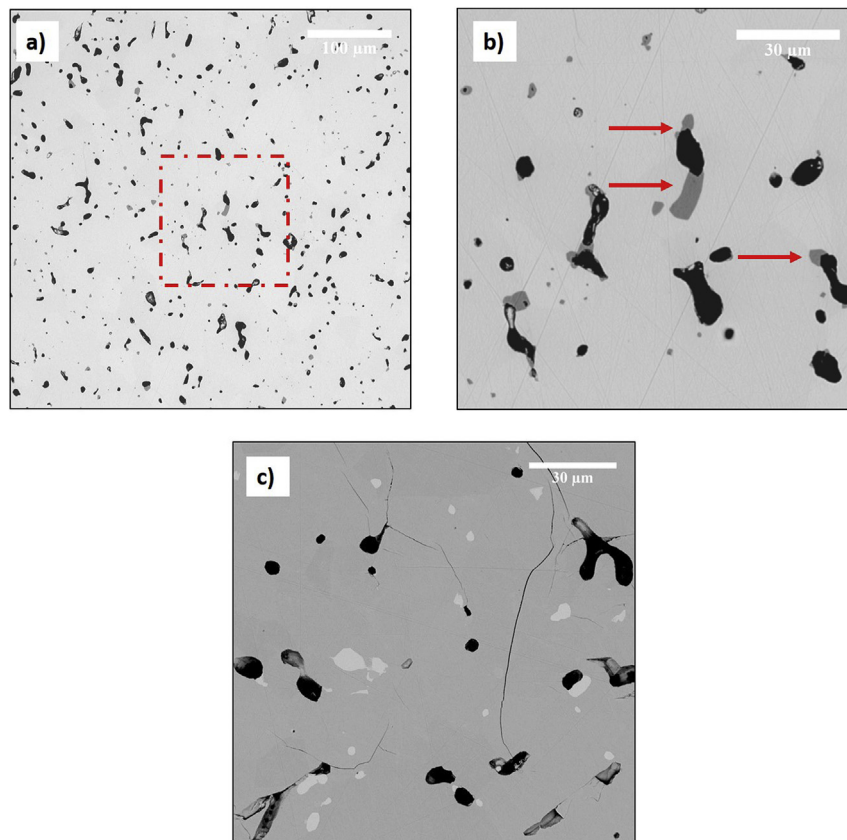

Fig. 2. Representative SEM images of U_3Si_2 set B (a,b) and U_3Si_5 (c). A higher magnification of the boxed region in a) is shown in b). Analysis of the U_3Si_2 set B samples identified regions of uranium and oxygen (red arrows in b) determined to be UO_2 by companion XRD analysis. Examination of U_3Si_5 microstructure as shown in c) clearly shows microcracking and the presence of a uranium-rich phase (white regions) previously identified as USi [6].
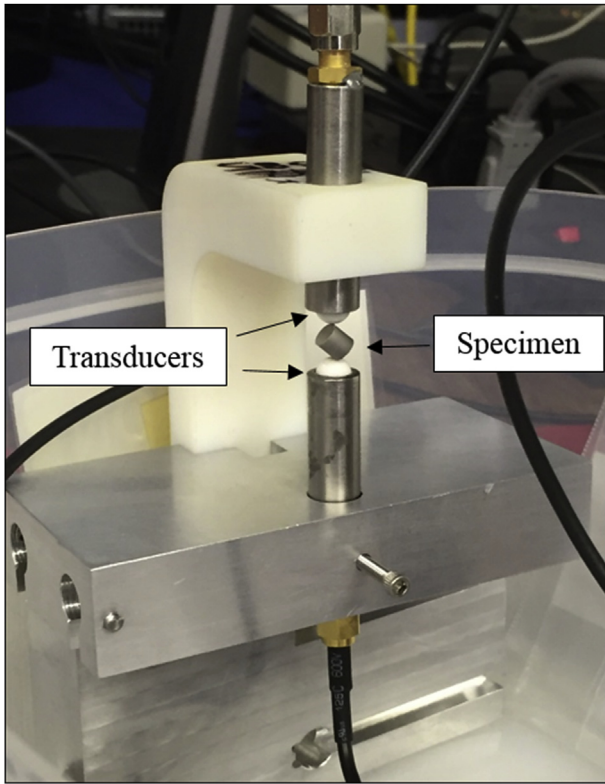
Fig. 3. Experimental set up of a RUS cylinder sample sandwiched between hemispherical Al_2O_3 wear plates, glued to the transducers.
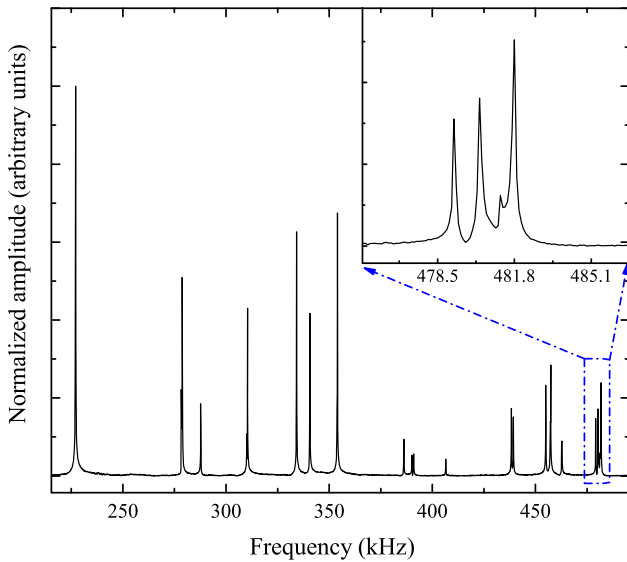

Fig. 4. Measured frequency response of a U_3Si_2 sample from 200 to 500 kHz.

mass of the specimens. A numerical approximation is used to predict the resonance spectrum of the specimen, and this approximation is then compared to the spectrum obtained experimentally. An iterative process is used to refine fitting parameters until the error falls below an acceptable limit. More details on the approach including its mathematical basis, strengths, and limitations can be found elsewhere [22,28].

For all samples included in this study, 15—30 resonances were obtained and a successful inversion was performed for all samples

[29,30]. The final inversion was within a 1% root mean square (RMS) error (the deviation between experimental and calculated resonance frequencies). Assuming a polycrystalline isotropic sample, there are two independent elastic constants C_{11} and C_{44}, making $C_{12} = C_{11}-2C_{44}$. The quality of fit resulting from the calculated frequencies justifies this approximation for polycrystalline material as characterized here. The shear modulus (G) corresponds to C_{44} and the bulk modulus (K) can then be calculated as:

$$K = \frac{C_{11} - 4C_{44}}{3} \tag{1}$$

Young's modulus (E) can be determined from:

$$E = C_{11} - \frac{2(C_{11} - 2C_{44})^2}{2C_{11} - 2C_{44}} \tag{2}$$

Finally, the Poisson's ratio (ν) corresponds to:

$$\nu = \frac{C_{11} - 2C_{44}}{2C_{11} - 2C_{44}} \tag{3}$$

3. Results and discussion

3.1. RUS measurements

Fig. 4 shows a typical resonance spectrum obtained for U_3Si_2. The mean values of the frequencies along with the observed and predicted mode frequencies are shown in Table 2. Good agreement is observed between the experimental and calculated resonance spectrum. The resonance structure is highly dependent on the cylinder dimensions, mass, porosity and oxygen impurities content between sets A and B. Amplitude depends on the modes obtained; since the masses of these samples are similar, no difference in amplitude were observed between set of samples.

Attempts were also made to analyze U_3Si_5 in a similar manner. However, poor resonance data was obtained despite multiple

Table 2
Comparison between the observed (f^{obs}) and predicted (f^{pre}) mode frequencies with error obtained for a U_3Si_2 sample.

Freq.#	(f^{obs})	(f^{pre})	%Error
1	227.090	225.640	−0.64
2	278.344	276.868	−0.53
3	278.842	276.868	−0.71
4	287.748	289.632	0.65
5	287.912	289.632	0.60
6	310.085	309.631	−0.15
7	310.430	309.631	−0.26
8	334.171	333.010	−0.35
9	340.572	341.273	0.21
10	340.702	341.273	0.17
11	353.855	353.779	−0.02
12	354.034	353.779	−0.07
13	386.204	388.632	0.63
14	390.140	390.292	0.04
15	390.953	390.292	−0.17
16	406.517	408.064	0.38
17	438.320	438.480	0.04
18	439.268	438.480	−0.18
19	454.970	451.281	−0.81
20	457.151	456.580	−0.12
21	457.367	456.580	−0.17
22	462.728	466.097	0.73
23	462.903	466.097	0.69
24	479.221	478.935	−0.06
25	480.159	480.466	0.06

attempts performed on several samples. The inadequate resonance data for all U_3Si_5 samples analyzed in this study indicate the low quality of the samples (see Fig. 2 c). This suggests that microcracking was present in the U_3Si_5 samples analyzed. Microcracking in U_3Si_5 samples at room temperature is consistent with existing thermophysical property measurements [6] and observations of oxidation behavior [31] for this compound. These previous investigations have attributed the microcracking to an elevated temperature phase transformation. Further work is needed to confirm or disprove this hypothesis.

3.2. Calculation of the elastic constants

The results of the elastic constants C_{11} and C_{44} along with the associated root mean square (RMS) values, are shown in Table 3. Assumed the average C_{44} value is 55.2±0.3 GPa and 52.3±0.2 GPa for set A and B, respectively while the average compressional modulus, C_{11}, value is 141.9±0.7 GPa for set A and 133.9±0.4 GPa for set B. Variation of C_{11} (6%) is slightly higher than the variation of C_{44} (5%) because C_{11} it is not as dependent on the resonant modes used for the fits. The fact that all U_3Si_2 samples resonate and show similar amplitude indicate the high quality of the samples.

Few studies have measured the elastic properties of U_3Si_2. Taylor et al. [32] determined the Young's modulus, E, 125±4 GPa and C_{44} and calculated the Poisson's ratio, ν, 0.185 by transverse acoustic measurements on U_3Si_2 98% sintered pellets. Shimizu [33] determined a value of 96±40 GPa for the elastic modulus of U_3Si_2 on induction arc-cast specimens using compression testing. However, the results from Shimizu exhibit considerably higher scatter. Shimizu also determined bulk modulus for U_3Si_2 on arc-cast specimens. The low value obtained 52.4 GPa may be due to cracking. Results obtained in this study are in a good agreement with Taylor and McMurtry data and are also within the uncertainty of Shimizu's results. However, more detailed comparison or discussion of the present results to these historic studies is challenged by the lack of chemical and microstructural characterization of U_3Si_2 in past works.

Table 4 shows a comparison of the elastic properties of U_3Si_2 and UO_2 collected in this study. The Young's modulus determined for UO_2 (96% theoretical density), 205.3 GPa, is in good agreement with literature values obtained for fully dense material by ultrasonic measurements, 204.7 GPa [34] and 223 GPa [9]. The effect of UO_2 content can be assessed by comparing the elastic properties of specimens from set A and set B. Porosity variation may affect the

Table 3
Elastic constants for U_3Si_2 sets A and B as determined in this study. A comparison to available literature data is provided for both experimentally and theoretically determined values from sources described in the text.

Sample	Ref.	C_{11} GPa	C_{44}, B GPa	K GPa	E GPa	ν	RMS %
A-1	a	142.0±0.6	55.1±0.3	68.5±0.4	130.4	0.183	0.392
A-2	a	142.1±1.0	55.0±0.5	68.8±0.7	130.2	0.185	0.742
A-3	a	141.8±0.6	55.7±0.4	67.6±0.5	131.1	0.177	0.554
A-4	a	142.1±0.6	55.2±0.2	68.5±0.3	130.5	0.183	0.359
A-5	a	141.5±0.7	55.0±0.3	68.2±0.4	129.9	0.182	0.496
B-6	a	136.3 ±0.4	52.8±0.2	66.0±0.3	125.1	0.184	0.259
B-7	a	131.6±0.5	51.0±0.2	63.6±0.3	120.7	0.184	0.342
	[32]·b		50.3		125±4	0.185	
	[33]·b				96±40		
	[37]·c		67.68		163.06		
	[38]·c	149	63	81	142.84		

a This study.
b From experimental results.
c From theoretical calculations.

Table 4
Summary of elastic property data collected in this study. The mean density of the sintered U_3Si_2 pellets for set A and B were about 94% and 92% respectively, while the density of UO_2 measured was 96% theoretical.

Elastic properties	UO_2	U_3Si_2- set A	U_3Si_2- set B
Shear Modulus, B (GPa)	77.9±0.1	55.2±0.3	52.3±0.2
Bulk Modulus, K (GPa)	187.6±0.8	68.3±0.5	64.3±0.3
Young's Modulus, E (GPa)	205.3±1.9	130.4±0.5	122.9±2.4
Poisson's ratio, ν	0.317±0.002	0.182±0.003	0.179±0.007

elastic moduli of the sintered pellets [35]. U_3Si_2 set B samples exhibit lower values of Young's modulus (120–125 GPa) compared with samples of the U_3Si_2 set A set with lower porosity (130–131 GPa). The increased porosity causes decrease of E [36].

It is noteworthy that the presence of UO_2 does not impact Young's modulus of a U_3Si_2 pellet in a manner related to the properties of bulk UO_2. If a simple rule of mixtures approximation is used, any appreciable fraction of UO_2 present in U_3Si_2 would increase Young's modulus of the bulk sample. However, the result obtained corresponds to the value calculated for a 92% U_3Si_2 material. Assessment of the measured and calculated elastic properties reported in Table 2 shows that all values measured here are not increased by the presence of UO_2. This result would only be expected to hold for relatively low volume contents of impurity phases.

Results obtained in this study are lower than theoretical mechanical data calculation for U_3Si_2 found by other authors in the literature [37,38] (see Table 3). The most obvious difference between the theoretical calculations and the experimental measurements collected in this work are the presence of both porosity and grain boundaries in the materials as measured. The presence of either would be expected to lower Young's modulus compared to fully dense, single crystal material. However, it is also possible that more complex behaviors of U_3Si_2 are not accounted for by the cited calculations.

3.3. Thermal stress evaluation

3.3.1. Model

As with most intermetallics, U_3Si_2 is a brittle material. Limited experimental data shows that U_3Si_2 is brittle [39] with a ductile behavior above 800°C [32]. The ratio G/K of the shear modulus divided by the bulk modulus is stated by Pugh as a simple estimator of the correlation between the ductile/brittle properties [40]. A material is considered brittle if $G/K > 0.5$. While originally conceived to describe the behavior of pure metals, its utility when applied to intermetallic and ceramic compounds has been demonstrated [41,42]. Therefore, according to Pugh's rule, U_3Si_2 is considered brittle at room temperature, with a ratio of G/K equal to 0.8. However, nuclear fuels are generally not asked to perform as a structural material. The future availability of RUS data at elevated temperatures, or use of other conventional mechanical testing methodologies, may clarify the ductile-to-brittle transformation temperature for U_3Si_2 based on this criterion.

At the beginning of the reactor operation, thermal expansion of the fuel results in pellet cracking due to the poor strength of the ceramic fuel in tension. This occurs prior to swelling or irradiation effects in the very early stage of reactor operation in pile. The fuel cracking phenomena, may be treated by thermoelastic theory [43].

The hoop stress due to the thermal gradient, σ, in a cylindrical pellet under elastic strain behavior is a function of q', the linear heat generation, and a number of thermophysical and thermomechanical material properties. Utilizing a rigid pellet assumption, where E is the elastic modulus of the fuel, α is the thermal expansion

coefficient, λ is the thermal conductivity, and ν is the Poisson's ratio, the hoop stress as a function of normalized radius is given by the following equation:

$$\sigma(r/R) = \frac{(E\alpha q)/(16\pi\lambda(1-\nu))}{\left(1-3(r/R)^2\right)} \qquad (4)$$

Equation (4) indicates compression of the fuel out to a fractional radius of 0.55 and tensile hoop stress thereafter. Although the radial temperature gradient in an operating fuel is significant, this approximation assumes temperature-independent properties to provide an approximation of the stress within the fuel.

Given the thermal expansion coefficient and thermal conductivity values obtained experimentally for U_3Si_2 [4] and UO_2 [24], thermal stress for both materials has been evaluated as a function of the fuel radius, where r/R is the fractional distance along the pellet's radius.

Experimental data of the fracture strength for the U_3Si_2 is not available, but a parameter that contains that properties that govern the resistance of a solid to failure by thermal stress can be expressed by:

$$M = \frac{\sigma_F(1-\nu)\lambda}{\alpha E} \qquad (5)$$

M is called the thermal shock resistance parameter [17]. The larger M is, the more resistant the fuel is to thermal stress failure. Thus, variables to affect M are inversely dependent; an increase in thermal conductivity or fracture strength or decrease in the Young's modulus and thermal expansion coefficient will increase M and improve resistance to cracking under extreme temperature gradients.

3.3.2. Analysis

The property values used for analysis of Equation (4) and Equation (5) and their sources are summarized in Table 5. According to Equation (4), an increase in thermal conductivity and/or decrease in thermal expansion coefficient values will reduce the magnitude of the stress at any point along the pellet radius. Fig. 5 highlights the impact of thermal conductivity on thermal stress, as the improved thermal conductivity offered by U_3Si_2 appreciably reduces stress compared to UO_2. This improvement is hypothesized to be even more significant as fuel is irradiated, since the thermal conductivity of U_3Si_2 is anticipated to degrade far less than UO_2 as a function of irradiation damage and burnup [4].

Analysis of the results plotted in Fig. 5 to assess the likelihood of fracture in U_3Si_2 is not possible at this time given the absence of mechanical property data for U_3Si_2. The flexural strength varies from 225.9 to 77.9 MPa in the range of 25—600°C. UO_2 has received wider attention with respect to its failure behavior, and at these low temperatures remains almost constant at 110 MPa [44]. Use of

Table 5
Parameters used for calculating pellet thermal stresses.

	T (°C)	Flexural Strength (MPa)	λ Wm^{-1}K^{-1}	E (GPa)	ν	α K^{-1}
U_3Si_2	25	86.2,[d] 225.9[c]	8.3[a]	130.4*	0.182*	16.1 × 10^{-6a}
	600	77.9[d]	15.6[a]			
UO_2	25	110[e]	9[b]	205.3*	0.317*	10.52 × 10^{-6b}
	600	110[e]	4.2[b]			

*This study.
 [a] J. White et al. [4].
 [b] J. White et al. [24].
 [c] Shimizu et al. [33].
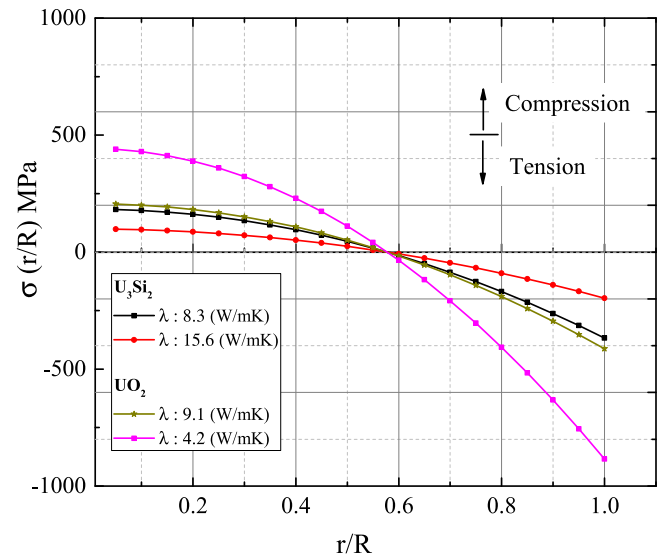 [d] Taylor et al. [32].
 [e] Evans et al. [44].

Fig. 5. Thermal stress induced by heat generation in U_3Si_2 and UO_2 as a function of the radius evaluated using Equation (4) and parameters in the text. Stresses are calculated using two different values for the thermal conductivity as shown in the legend. These correspond to their unirradiated thermal conductivity values at 25 and 600 °C.

these values as inputs to Equation (5) yields M of 472—1541 W/m and 87 W/m for U_3Si_2 and UO_2 respectively. This parameter suggests that, even when the lowest existing fracture strength data for U_3Si_2 is used, it will have significantly greater resistance to fracture under thermal gradients than UO_2. However, further experimental data need to be collected to confirm the U_3Si_2 thermal stress analysis modeling.

4. Conclusions

Mechanical testing was carried out via RUS to determine the bulk and shear modulus of U_3Si_2. The C_{44} is 55.2±0.3 GPa, with a bulk modulus of 68.3±0.5 GPa. Preliminary assessment did not show a significant impact of UO_2 impurities on the mechanical properties of monolithic U_3Si_2. The results obtained suggest that a higher density U_3Si_2 sample leads to an increase on the elastic values as expected. The measurement of these properties allowed a basic analysis of the maximum thermal stress and estimation of the thermal shock resistance of U_3Si_2. A comparison of U_3Si_2 to UO_2 using the available mechanical properties suggest that it will be more resistant to cracking than UO_2 during reactor startup and core power maneuvers.

Acknowledgments

References

[1] J.M. Harp, P.A. Lessing, R.E. Hoggan, Uranium silicide pellet fabrication by powder metallurgy for accident tolerant fuel evaluation and irradiation, J. Nucl. Mater 466 (2015) 728—738.

[2] A. Nelson, J. White, D. Byler, J. Dunwoody, J. Valdez, K. Mcclellan, Overview of properties and performance of uranium-silicide compounds for light water reactor applications, Trans. Am. Nucl. Soc. 110 (2014) 987–989.

[3] J. White, A. Nelson, D. Byler, J. Valdez, K. McClellan, Thermophysical properties of U_3Si to 1150 K, J. Nucl. Mater 452 (13) (2014) 304–310.

[4] J. White, A. Nelson, J. Dunwoody, D. Byler, D. Safarik, K. McClellan, Thermophysical properties of U_3Si_2 to 1773 k, J. Nucl. Mater 464 (2015) 275–280.

[5] J. White, A. Nelson, J. Dunwoody, D. Byler, K. McClellan, Thermophysical properties of USi to 1673 k, J. Nucl. Mater 471 (2016) 129–135.

[6] J. White, A. Nelson, D. Byler, D. Safarik, J. Dunwoody, K. McClellan, Thermophysical properties of U_3Si_5 to 1773 k, J. Nucl. Mater 456 (2015) 442–448.

[7] H. Matzke, Indentation Fracture and Mechanical Properties of Ceramic Fuels and Glasses, Applied Research Reports, Harwood, 1987.

[8] D. Laux, W. de Weerd, D. Papaioannou, S. Kitajima, V. Rondinella, G. Despaux, Scanning acoustic microscope for mechanical characterization and density estimation of irradiated nuclear fuel, Prog. Nucl. Energy 72 (2014) 63–66 symposium E-MRS 2013. Scientific basis of the nuclear fuel cycle.

[9] D. Laux, D. Baron, G. Despaux, A. Kellerbauer, M. Kinoshita, Determination of high burn-up nuclear fuel elastic properties with acoustic microscopy, J. Nucl. Mater. 420 (1) (2012) 94–100.

[10] K. Phani, D. Sanyal, A. Sengupta, Estimation of elastic properties of nuclear fuel material using longitudinal ultrasonic velocity a new approach, J. Nucl. Mater 366 (12) (2007) 129–136.

[11] J.-M. Gatt, Y. Monerie, D. Laux, D. Baron, Elastic behavior of porous ceramics: application to nuclear fuel materials, J. Nucl. Mater 336 (23) (2005) 145–155.

[12] S. Yamanaka, S. Yoshida, K. Kurosaki, M. Uno, K. Yamamoto, T. Namekawa, Mechanical properties of $(U,Ce)O_2$ with and without Nd or Zr, J. Alloy Comp 327 (12) (2001) 281–284.

[13] S. Aravindan, S. Jalaldeen, P. Chellapandi, N. Swaminathan, Yield behavior of porous nuclear fuel $(UO)_2$, Mech. Adv. Mater. Struct. 23 (10) (2016) 1149–1162.

[14] M. Pujol, M. Idiri, L. Havela, S. Heathman, J. Spino, Bulk and youngs modulus of doped (UO_2) by synchrotron diffraction under high pressure and knoop indentation, J. Nucl. Mater 324 (23) (2004) 189–197.

[15] C.O. Smith, Thermal stresses and their significance in nuclear fuel elements, J. Am. Soc. Nav. Eng. 72 (3) (1960) 393–400.

[16] High burnup performance of annular UO_2 fuel with inter-pellet graphite discs, J. Nucl. Mater 126 (2) (1984) 177–180.

[17] D. Olander, Fundamental Aspects of Nuclear Reactor Fuel Elements, 1976.

[18] A. Wolfenden, Dynamic Elastic Modulus Measurements in Materials, ASTM, 1990.

[19] J. Kim, K.-Y. Jhang, Non-contact measurement of elastic modulus by using laser ultrasound, Int. J. Precis. Eng. Manuf. 16 (5) (2015) 905–909.

[20] R.G. Leisure, F.A. Willis, Resonant ultrasound spectroscopy, J. Phys. Condens. Matter 9 (28) (1997) 6001.

[21] A. Migliori, T.W. Darling, Resonant ultrasound spectroscopy for materials studies and non-destructive testing, Ultrasonics 34 (25) (1996) 473–476 proceedings of Ultrasonics International 1995.

[22] A. Migliori, J.D. Maynard, Implementation of a modern resonant ultrasound spectroscopy system for the measurement of the elastic moduli of small solid specimens, Rev. Sci. Instrum. 76 (12) (2005) 121–301.

[23] K. Remschnig, T.L. Bihan, H. Nol, P. Rogl, Structural chemistry and magnetic behavior of binary uranium silicides, J. Solid State Chem. 97 (2) (1992) 391–399.

[24] J. White, A. Nelson, Thermal conductivity of UO_{2+x} and U_4O_{9y}, J. Nucl. Mater 443 (13) (2013) 342–350.

[25] W.H. Zachariasen, Crystal chemical studies of the 5f-series of elements. VIII. Crystal structure studies of uranium silicides and of $CeSi_2$, $NpSi_2$, and $PuSi_2$, Acta Crystallogr. 2 (2) (1949) 94–99.

[26] C.A. Schneider, W.S. Rasband, K.W. Eliceiri, NIH image to ImageJ, Nat. Methods 9 (2012) 671–675.

[27] C. Payan, T.J. Ulrich, P.Y.L. Bas, T. Saleh, M. Guimaraes, Quantitative linear and nonlinear resonance inspection techniques and analysis for material characterization: application to concrete thermal damage, J. Acoust. Soc. Am. 136 (2) (2014) 537–546.

[28] A. Migliori, J. Sarrao, W.M. Visscher, T. Bell, M. Lei, Z. Fisk, R. Leisure, Resonant ultrasound spectroscopic techniques for measurement of the elastic moduli of solids, Phys. B Condens. Matter 183 (1) (1993) 1–24.

[29] J. Maynard, Resonant ultrasound spectroscopy, Phys. Today 49 (1) (1996) 26–31.

[30] J. Moré, The Levenberg-Marquardt algorithm: implementation and theory, in: G.A. Watson (Ed.), Numerical Analysis, Vol. 630 of Lecture Notes in Mathematics, Springer Berlin Heidelberg, 1978, pp. 105–116.

[31] E.S. Wood, J. White, A. Nelson, Oxidation behavior of U-Si compounds in air from 25 to 1000C, J. Nucl. Mater. 484 (2017) 245–257.

[32] K. Taylor, C. McMurtry, Synthesis and Fabrication of Refractory Uranium Compounds, ORO-400, 1961.

[33] H. Shimizu, The Properties and Irradiation Behavior of U_3Si_2, Tech. Rep. Tech. Rep. NAA-SR-10621, Atomics International, July 1965.

[34] A. Padel, C. De Novion, Constantes elastiques des carbures, nitrures et oxydes d'uranium et de plutonium, J. Nucl. Mater 33 (1969) 40–51.

[35] R.W. Rice, Effects of inhomogeneous porosity on elastic properties of ceramics, J. Am. Ceram.Soc. 58 (9–10) (1975) 458–459.

[36] J. Kováčik, Correlation between young's modulus and porosity in porous materials, J. Mater. Sci. Lett. 18 (13) (1999) 1007–1010.

[37] T. Wang, N. Qiu, X. Wen, Y. Tian, J. He, K. Luo, X. Zha, Y. Zhou, Q. Huang, J. Lang, S. Du, First-principles investigations on the electronic structures of U_3Si_2, J. Nucl. Mater 469 (2016) 194–199.

[38] M.J. Noordhoek, T.M. Besmann, D. Andersson, S.C. Middleburgh, A. Chernatynskiy, Phase equilibria in the U-Si system from first-principles calculations, J. Nucl. Mater 479 (2016) 216–223.

[39] A. Kaufmann, B. Cullity, G. Bitsianes, Phase equilibria in the U-Si system from first-principles calculations, J. Metals (1957) 23–27, 23–27.

[40] S. Pugh, Relations between the elastic moduli and the plastic properties of polycrystalline pure metals, Philos. Mag. 45 (367) (1954) 823–843.

[41] K. Trachenko, J.M. Pruneda, E. Artacho, M.T. Dove, How the nature of the chemical bond governs resistance to amorphization by radiation damage, Phys. Rev. B 71 (2005) 184104.

[42] K. Trachenko, M.T. Dove, E. Artacho, I.T. Todorov, W. Smith, Atomistic simulations of resistance to amorphization by radiation damage, Phys. Rev. B 73 (2006) 174207.

[43] T.L. Van Brutzel, R. Dingreville, Nuclear Fuel Deformation Phenomena, Nuclear Energy Agency of the OECD (NEA), 2015.

[44] A. Evans, R. Davidge, The strength and fracture of stoichiometric polycrystalline UO_2, J. Nucl. Mater 33 (3) (1969) 249–260.

[45] R. Fritsche, C. Sussieck-Fornefeld, Min.-Petr. Inst., Univ. Heidelberg, Germany, ICDD Grant-in-Aid, 1988.